

Low-Dilution Limit of $Zn_{1-x}Mn_xGeAs_2$: electrical and magnetic properties

L. Kilanski,^{1,*} K. Szalowski,² R. Szymczak,¹ M. Górska,¹ E. Dynowska,¹ P. Aleshkevych,¹ A. Podgórní,¹ A. Avdonin,¹ W. Dobrowolski,¹ I. V. Fedorchenco,³ and S. F. Marenkin³

¹*Institute of Physics, Polish Academy of Sciences, Al. Lotników 32/46, 02-668 Warsaw, Poland*

²*Department of Solid State Physics, Faculty of Physics and Applied Informatics, University of Łódź, ul. Pomorska 149/153, 90-236 Łódź, Poland*

³*Kurnakov Institute of General and Inorganic Chemistry RAS, 119991 Moscow, Russia*

(Dated: December 3, 2024)

We present the studies of electrical transport and magnetic interactions in $Zn_{1-x}Mn_xGeAs_2$ crystals with low Mn content $0 \leq x \leq 0.043$. We show that the ionic-acceptor defects are mainly responsible for the strong *p*-type conductivity of our samples. We found that the negative magnetoresistance (MR) with maximum values of about -50% is related to the weak localization phenomena. The magnetic properties of $Zn_{1-x}Mn_xGeAs_2$ samples show that the random Mn-distribution in the cation sites of the host lattice occurs only for the sample with the lowest Mn-content, $x = 0.003$. The samples with higher Mn-content show a high level of magnetic frustration. Nonzero Curie-Weiss temperature observed in all our samples indicates that weak ferromagnetic (for $x = 0.003$) or anti-ferromagnetic (for $x > 0.005$) interactions with $|\Theta| < 3$ K are present in this system. The RKKY model, used to estimate the Mn-hole exchange integral J_{pd} for the diluted $Zn_{0.997}Mn_{0.003}GeAs_2$ sample, makes possible to estimate the value of $J_{pd} = (0.75 \pm 0.09)$ eV.

PACS numbers: 72.80.Ga, 75.30.Hx, 75.30.Et, 75.50.Pp

Keywords: semimagnetic-semiconductors; magnetic-impurity-interactions, exchange-interactions

I. INTRODUCTION

Complex diluted magnetic semiconductors (DMS) are a subject of considerable interest in the recent years since they offer many advantages over classical II-VI and III-V materials.^{1,2} Ferromagnetic semiconductors with the Curie temperature, T_C , greater than room temperature, are needed for practical applications. However, most of the literature reports about the magnetic properties of DMS systems show the Curie temperatures much lower than 300 K, which makes these compounds of a little use for practical applications. The absence of room temperature ferromagnetic DMS systems creates the need for the development of new compounds fulfilling technological requirements.

Recently II-IV-V₂ chalcopyrite semiconductors doped with transition metal ions have become a subject of considerable interest due to the appearance of room temperature ferromagnetism, creating the possibilities of utilizing them in spintronics.^{3,4} It is known that the short-range magnetic interactions connected with the presence of magnetic clusters are responsible for high-temperature ferromagnetism in these alloys.⁵⁻⁷ Among many experimental investigations showing ferromagnetism with large Curie temperatures due to short-range ordering there seems to be a shortage of studies devoted to low-dilution limits in which itinerant ferromagnetism might be induced. The possibility to control the magnetic properties of the material via changes in their electronic transport properties needed to fulfil the main aim of semiconductor spintronics,⁸ will be possible only when homogeneous materials will be technologically mastered and properly understood.

In the present work we investigate magnetotransport

and magnetic properties of $Zn_{1-x}Mn_xGeAs_2$ crystals with low Mn content x varying in the range from 0 to 0.042. The present work extends our earlier research devoted to both nanocomposite $ZnGeAs_2:MnAs$ samples⁵⁻⁷ and homogeneous $Zn_{1-x}Mn_xGeAs_2$ crystals.^{9,10} The low dilution Mn-alloying improves the structural quality of the samples allowing one to study long-range carrier mediated magnetic interactions in this system. Since $Zn_{1-x}Mn_xGeAs_2$ crystals are *p*-type semiconductors with large solubility of Mn-ions, the induction of the carrier-mediated-ferromagnetism seems to be a realistic aim. In order to understand the Mn-incorporation into this alloy the complexity of the magnetic interactions between Mn-ions needs to be understood.

II. BASIC CHARACTERIZATION

We present the studies of bulk $Zn_{1-x}Mn_xGeAs_2$ crystals grown using a direct fusion method from high purity $ZnAs_2$, Ge, and Mn powders taken in stoichiometric ratios.¹¹ The growth was performed at a temperature of about 1200 K. Mn-doped crystals were cooled from the growth temperature down to 300 K with a relatively high speed (about 5-10 K/s) in order to improve the homogeneity of the samples and prevent Mn clustering.

The chemical composition of the samples was determined using energy dispersive x-ray fluorescence method (EDXRF). A typical relative uncertainty of this method was about 10%. The as-grown crystals were cut into slices with thickness of about 1.5 mm prior to their structural characterization. The EDXRF analysis shows that our samples have Mn content x changing in the range from 0 to 0.042. Moreover, it must be emphasized, that

within our measurement accuracy all the studied crystals have the correct stoichiometry of Zn:Ge:As equal to 1:1:2.

High resolution x-ray diffraction method (HRXRD) was used to investigate the structural properties of $Zn_{1-x}Mn_xGeAs_2$ crystals. Measurements were performed with the use of multipurpose X'Pert PRO MPD, Panalytical diffractometer with Cu $K\alpha_1$ radiation with wavelength $\lambda = 1.5406 \text{ \AA}$, configured for Bragg-Brentano diffraction geometry and equipped with a strip detector and an incident-beam Johansson monochromator. In order to increase the accuracy and quality of the diffraction patterns the data acquisition in each individual measurement was done over several hours. The indexing procedure of measured diffraction patterns as well as calculations of the lattice parameters were performed using SCANIX 2.60PC program.¹²

The analysis of the HRXRD results allows us to identify two cubic disordered zincblende phases with $a = 5.6462 \pm 0.0002 \text{ \AA}$ and $a = 5.9055 \pm 0.0007 \text{ \AA}$ for the pure $ZnGeAs_2$ crystal. The addition of a small quantity of Mn ($x = 0.003$) to the $Zn_{1-x}Mn_xGeAs_2$ alloy results in stabilization of the tetragonal chalcopyrite structure with $a = 5.6751 \pm 0.0002 \text{ \AA}$ and $c = 11.1534 \pm 0.0005 \text{ \AA}$. Additionally, the cubic zincblende phase is observed in $Zn_{1-x}Mn_xGeAs_2$ sample with $x = 0.003$ with $a = 5.6471 \pm 0.0004 \text{ \AA}$. Further increase of Mn content above $x = 0.003$ results in a change of the main crystallographic phase of the alloy back to the cubic disordered zincblende structure. The lattice parameters determined for $Zn_{1-x}Mn_xGeAs_2$ crystals with $x > 0.01$ are similar to those reported for pure $ZnGeAs_2$ sample. The coexistence of disordered cubic zincblende and chalcopyrite tetragonal structures is justified by the phase diagram of the ternary Zn-Ge-As system¹³ in which both compounds lie on the same line connecting Ge and $ZnAs_2$. It must be emphasized, that diffraction patterns for both disordered zincblende and chalcopyrite structures (see Ref. 13) are located very close to each other and it was possible to distinguish between them only with the use of state-of-the-art diffractometer. We want to emphasize that all our samples have almost perfect stoichiometry of $ZnGeAs_2$ compound, as determined with the use of the EDXRF technique. It is hence evident, that our alloy is based on $ZnGeAs_2$ compound, but the presence of the cubic disordered zincblende structure is a signature of a large chemical disorder of the alloy, widely observed in ternary chalcopyrite systems,¹⁴ reflecting a mixing of the Zn and Ge atoms in the cation sublattice.

III. MAGNETOTRANSPORT DATA

In order to obtain information about fundamental electrical properties of the studied $Zn_{1-x}Mn_xGeAs_2$ alloy, temperature dependent magnetotransport measurements were performed. We have used the superconducting magnet with maximum magnetic field equal to $B = 13 \text{ T}$ and

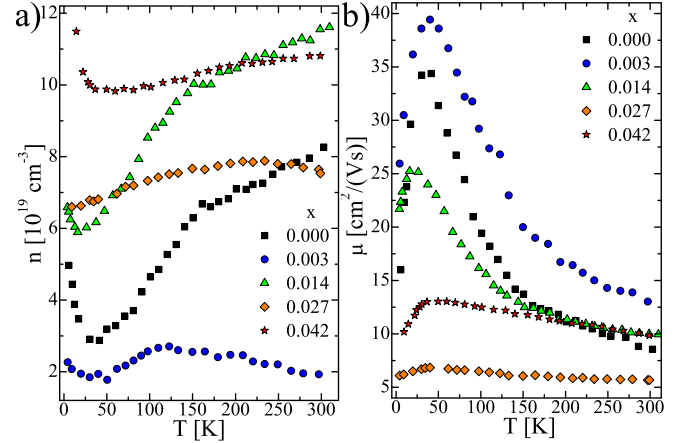


FIG. 1. The magnetotransport data including (a) Hall carrier concentration and (b) carrier mobility as a function of temperature for $Zn_{1-x}Mn_xGeAs_2$ samples containing different amount of Mn (see legend).

a sweep speed of about 0.5 T/min, equipped with the cryostat allowing the control of the temperature of the sample in the range of $1.4 \leq T \leq 300 \text{ K}$. The samples, cut to size of about $1 \times 1 \times 10 \text{ mm}$, were etched and cleaned before making electrical contacts. The contacts were made with the use of gold wire and indium solder. The ohmic behavior of each contact pair was checked prior to proper measurements. The magnetoresistance and the Hall effect were measured simultaneously at selected temperatures.

A. Basic magnetotransport characterization

Initially, we measured the temperature dependence of the resistivity parallel to the current direction, ρ_{xx} , in the absence of an external magnetic field. Our results show, that in the case of all the samples a metallic $\rho_{xx}(T)$ dependencies are observed, the behavior characteristic for degenerate semiconductors, i.e., an increase of the resistivity with an increasing temperature. It indicates that the carrier transport in the studied samples is not due to thermal activation of band carriers. It is evident, that defect states have major influence on the conductivity of this alloy. The characteristic feature observed for all investigated samples is the existence of a shallow minimum in $\rho_{xx}(T)$ dependence at temperatures below 50 K. The existence of the minimum in $\rho_{xx}(T)$ dependence is likely to be related to the carrier scattering on the paramagnetic ions. Above $T = 50 \text{ K}$ the resistivity ρ_{xx} is an increasing, nearly linear function of the temperature.

The Hall effect measured as a function of temperature allows us to determine the temperature dependence of the Hall carrier concentration n in all our samples (see Fig. 1a). The results show that all our $Zn_{1-x}Mn_xGeAs_2$ crystals have a strong *p*-type conductivity with relatively high carrier concentration changing in the range of

$10^{19} \leq n \leq 10^{20} \text{ cm}^{-3}$. High concentration of conducting holes in this material is probably due to the existence of a large number of negatively charged Zn or Ge vacancy type defects and possibly other non-open-volume negatively charged defects. Inspection of results gathered in Fig. 1a shows that the Hall carrier concentration increases from $6 \times 10^{19} \text{ cm}^{-3}$ in the ZnGeAs_2 sample with disordered zincblende structure to $8 \times 10^{19} \text{ cm}^{-3}$ in the $\text{Zn}_{1-x}\text{Mn}_x\text{GeAs}_2$ sample with $x = 0.003$ and the chalcopyrite structure. Such an increase of the carrier concentration seems to be connected with thermodynamics of crystal growth which induced higher amount of point defects in the disordered zincblende structure crystal then that of chalcopyrite crystal. The higher concentration of electrically active defects resulted in an increase of the Hall carrier concentration. A general increase in the carrier concentration from $8 \times 10^{19} \text{ cm}^{-3}$ up to $11 \times 10^{19} \text{ cm}^{-3}$ is observed in the studied samples with an increase in the amount of Mn in the alloy from $x = 0$ up to 0.042, respectively. The noticeable increase in the concentration of conducting holes indicates poor Mn allocation in the crystal lattice, which leads to the formation of vacancy type or interstitial point defects likely to be electrically active.

The Hall carrier concentration is a decreasing function of temperature at $T < 50$ K for most of the studied samples, while at $T > 50$ K the trend in the $n(T)$ dependence is opposite. Negative slope of $n(T)$ dependence at $T < 50$ K is a signature of a high ionic scattering mechanism involved in the carrier scattering at low temperatures. On the other hand, a positive slope of $n(T)$ dependence at $T > 50$ K is a signature that defect states responsible for metallic $\rho_{xx}(T)$ dependence are likely to be electrically active and being thermally activated are a source of conducting holes in our samples.

The temperature dependent resistivity and the Hall effect data can be used to calculate the temperature dependence of the Hall mobility, $\mu = (e \cdot n \cdot \rho_{xx})^{-1}$, where e is the elementary charge. The calculated $\mu(T)$ dependence for all our $\text{Zn}_{1-x}\text{Mn}_x\text{GeAs}_2$ samples is presented in Fig. 1b. In all samples the $\mu(T)$ dependence has a maximum at $T < 50$ K. Such a feature is characteristic for charged impurity scattering mechanism being important in the conduction of the material. At a maximum of the $\mu(T)$ dependence the carrier mobility reflects the superposition of a weak lattice and phonon scattering processes. At temperatures higher than 50 K the $\mu(T)$ dependence is a decreasing function of temperature, which is a feature characteristic for phonon scattering mechanism. The highest value of the Hall carrier mobility, $\mu \approx 40 \text{ cm}^2/(\text{V}\cdot\text{s})$, is observed in the chalcopyrite $\text{Zn}_{0.997}\text{Mn}_{0.003}\text{GeAs}_2$ sample (at $T \approx 50$ K) indicating, that the lattice scattering and the concentration of electrically active defects is for this particular sample the smallest in the entire series. A decrease in the maximum carrier mobility from $35 \text{ cm}^2/(\text{V}\cdot\text{s})$ down to about $8 \text{ cm}^2/(\text{V}\cdot\text{s})$ with the increase of Mn content in the samples is observed. It is a direct signature, that the alloca-

tion of Mn in the ZnGeAs_2 lattice was far from perfect and induced charged defects in the material.

B. High Field Magnetotransport

The isothermal magnetoresistance (MR) and the Hall effect measurements were performed for all our $\text{Zn}_{1-x}\text{Mn}_x\text{GeAs}_2$ samples. The $\rho_{xx}(B)$ curves were obtained by averaging the results for positive and negative current. For a simple data presentation the $\rho_{xx}(B)$ curves at different temperatures were normalized to the zero-field resistivity value ρ_0 by using the following relation: $\Delta\rho_{xx}/\rho_{xx}(0) = (\rho_{xx}(B) - \rho_{xx}(B = 0))/\rho_{xx}(B = 0)$. In this manner, we calculated a number of isothermal magnetoresistance curves for each of the samples, obtained at various temperatures $T < 300$ K.

It should be noted, that MR for nonmagnetic ZnGeAs_2 crystal is positive and is proportional to the square of the magnetic field for $1.4 < T < 300$ K. This effect can be clearly associated with the classical magnetoresistance due to the orbital motion of carriers in a magnetic field. Moreover, in the ZnGeAs_2 sample at low temperatures there are no other contributions to the MR, such as the weak localization of carriers on defect states.¹⁵

The results of the magnetoresistance measurements for selected $\text{Zn}_{1-x}\text{Mn}_x\text{GeAs}_2$ samples performed at several stabilized temperatures are presented in Fig. 2. The results presented in Fig. 2 indicate that the addition of a small quantity of Mn to the $\text{Zn}_{1-x}\text{Mn}_x\text{GeAs}_2$ alloy results in a drastic change of the MR behavior with respect to the nonmagnetic ZnGeAs_2 crystal. The obtained results show a negative MR for our samples, present at temperatures lower than 30 K. Magnetoresistance in $\text{Zn}_{1-x}\text{Mn}_x\text{GeAs}_2$ samples with $x \leq 0.042$, studied in this paper have a different shape and the amplitude of the order of magnitude higher than that studied in Ref. 9 ($\text{Zn}_{0.947}\text{Mn}_{0.053}\text{GeAs}_2$ sample of similar concentration and mobility of carriers at $T = 1.4$ K). It is therefore clear that in the case of currently studied samples the magnetoresistance should be associated with a different mechanism than the spin-disorder scattering process.^{9,16}

The addition of a small quantity ($x = 0.003$) of Mn to the $\text{Zn}_{1-x}\text{Mn}_x\text{GeAs}_2$ alloy results in a drastic change of the MR with respect to the nonmagnetic ZnGeAs_2 sample. The chalcopyrite $\text{Zn}_{1-x}\text{Mn}_x\text{GeAs}_2$ sample with $x = 0.003$ shows negative MR with maximum value of about -50% at $T = 1.42$ K, slowly decreasing with the temperature to about 0.2% at $T = 20$ K. The MR at $T > 30$ K does not show any signatures of negative contribution and we can observe only a small positive contribution to the MR (with values less than 1%), proportional to the square of the magnetic field and slowly decreasing as a function of temperature. The positive MR at $T > 30$ K is caused by the orbital motion of conducting carriers in the presence of the external magnetic field.

The MR curves for our disordered zincblende $\text{Zn}_{1-x}\text{Mn}_x\text{GeAs}_2$ samples with $x \geq 0.014$ show much

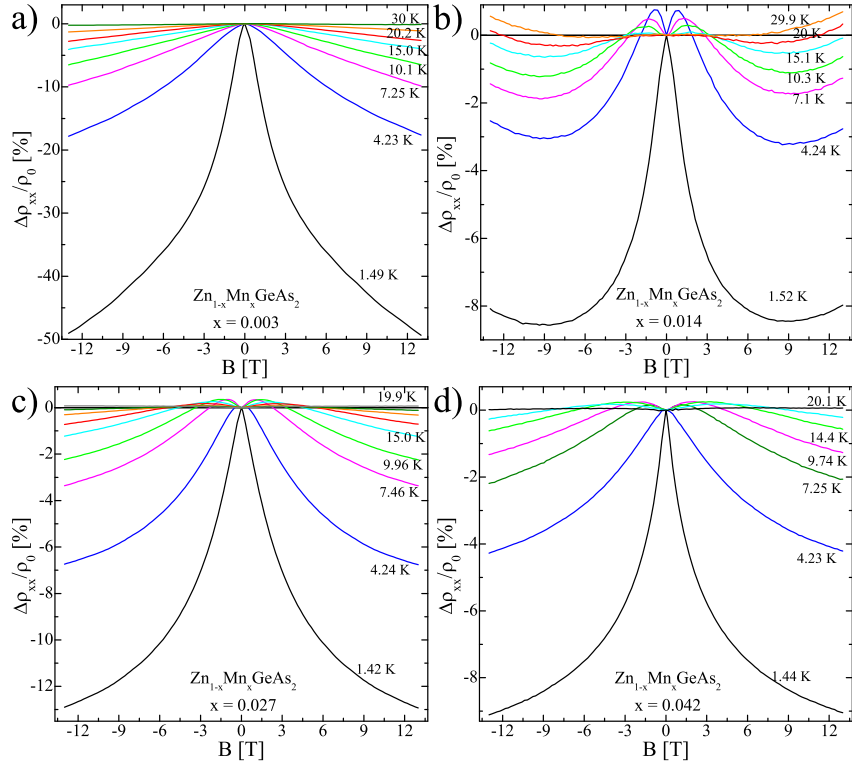


FIG. 2. The magnetoresistance curves obtained experimentally at different temperatures for $\text{Zn}_{1-x}\text{Mn}_x\text{GeAs}_2$ samples with different chemical composition.

smaller amplitudes (almost an order of magnitude lower) with respect to the chalcopyrite $\text{Zn}_{0.997}\text{Mn}_{0.003}\text{GeAs}_2$ sample. The maximum amplitude of negative MR equals 13% for the sample with $x=0.027$ at $T \approx 1.4$ K. Moreover, at low magnetic fields and at temperatures higher than 2 K we observe a positive contribution to the MR scaling with the square of the magnetic field, caused by the orbital MR.

We performed the scaling analysis of the negative MR observed in our samples at temperatures lower than 30 K. The scaling analysis to $\Delta\rho_{xx}/\rho_0 \propto B^m$ proportionality, where m is the scaling factor, shows, that the MR results for all our samples can be fitted with a good accuracy with the values of scaling factor around $0.6 \leq m \leq 0.8$. The value of the exponent m carries information about possible physical mechanism of the negative MR. The Moriya-Kawabata spin-fluctuation theories^{17,18} predict that the negative magnetoresistance should scale with $m=1$ and 2 for weakly and nearly ferromagnetic metals, respectively. Since the m values for our samples are lower than the above values we can exclude the spin-fluctuations from being the main physical mechanism responsible for the observed negative MR. Moreover, the dependence of the MR on the magnetization M normalized to the saturation magnetization M_S (M/M_S) is neither square nor cubic. It is another signature that the negative MR for our $\text{Zn}_{1-x}\text{Mn}_x\text{GeAs}_2$ samples originates

from processes that are not directly related with magnetic impurity scattering.

Theories of quantum corrections to the conductivity predict that weak localization (WL) phenomena can be responsible for negative MR present in many different disordered metals and semiconductors at low temperatures.²⁵ Localization shortens the mean free path of the carriers and gives rise to mobility edge in the valence band. The product k_{FL} , where k_F is the quasi-Fermi wave vector and l is the mean free path, reflects the degree of the disorder and localization in a material. For $k_{FL} \sim 1$ the disorder and electron localization are strong and the conducting holes cannot be thermally activated to the valence band, where they could diffuse thorough the crystal. The magnetic field and the presence of magnetic impurities destroys carrier localization allowing carriers to diffuse. Experimentally, it is visible as negative MR. The negative MR, caused by the WL in the presence of spin-orbit interaction and magnetic impurity scattering is predicted to show complex behavior. A number of different corrections has to be considered to fit the experimental MR results.²⁶ The k_{FL} factor at $T < 30$ K for all our samples indicating that the localization is strong. The theories of MR due to WL predict a presence of both positive (at low magnetic fields) and negative MR for low diffusivity systems ($0.5 \text{ cm}^2/\text{s}$). Moreover, the MR in our samples decreases with increas-

ing the average Mn content, x , and the related effective Mn content $x_{\bar{Mn}}$ derived from susceptibility and magnetization data. Thus, the observed MR is not related to magnetic impurity scattering mechanism that would lead to MR proportional to the amount of magnetic impurities in the crystal. WL is known to be destroyed by the presence of magnetic impurities in the material. Therefore, the destruction of the WL by the presence of an increasing number of magnetic impurities in the crystals explains the observed MR in the $Zn_{1-x}Mn_xGeAs_2$ samples with $x > 0.003$.

IV. MAGNETIC PROPERTIES

Magnetic properties of the $Zn_{1-x}Mn_xGeAs_2$ samples are studied by means of both ac and dc magnetometry. The mutual inductance method, employed into the LakeShore 7229 susceptometer/magnetometer system was used in order to determine the temperature dependencies of the ac magnetic susceptibility. The high field magnetization was measured with the use of Quantum Design XL-5 Magnetometer.

A. Low field results

The temperature dependence of the ac magnetic susceptibility was measured in the temperature range $4.3 \leq T \leq 180$ K. During the measurement the sample was put into the alternating magnetic field having amplitude $H_{AC} = 10$ Oe and frequency $f = 625$ Hz. The results in the form of the temperature dependences of the inverse of the real part of the magnetic susceptibility $(Re(\chi_{AC}))^{-1}(T)$ obtained in the case of several $Zn_{1-x}Mn_xGeAs_2$ samples having different Mn-content are showed in Fig. 3. As we can see all the samples showed paramagnetic Curie-Weiss behavior of the $(Re(\chi_{AC}))^{-1}(T)$ at temperatures between $4.3 \leq T \leq 30$ K. In II-IV-V₂ DMSs, we can distinguish two major components determining their magnetic properties. The first is the paramagnetic component introduced by Mn²⁺ ions with half filled 3d⁵ shell in the ground state with $S = 5/2$. The second term is the diamagnetic one originating from the nonmagnetic host lattice and substitutional diamagnetic ions. However, at higher temperatures, one can see the deviation of the $(Re(\chi_{AC}))^{-1}(T)$ from a paramagnetic temperature dependence towards lower values. It indicates the existence of an additional, temperature independent term in the $(Re(\chi_{AC}))^{-1}(T)$ curves. The Van-Vleck paramagnetism can be a source of the additional term in the magnetic susceptibility. Such effect with the susceptibility values around 10^{-7} emu/g was observed in $Cd_{1-x}Co_xSe$.²⁷ However, in our samples the additional susceptibility is about the order of magnitude higher. The additional susceptibility in our samples can be associated with the presence of magnetic ions coupled by the short range magnetic in-

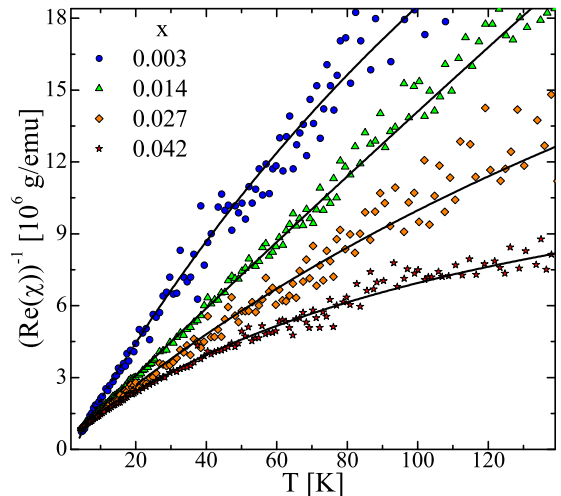


FIG. 3. The inverse of the magnetic susceptibility as a function of temperature for $Zn_{1-x}Mn_xGeAs_2$ samples containing different amount of Mn (see legend).

teractions.

The temperature dependence of the inverse of the magnetic susceptibility $(Re(\chi_{AC}))^{-1}(T)$ for the temperatures well above the Curie-Weiss temperature can be fitted with the use of the modified Curie-Weiss law in the form:

$$\chi(T) = \frac{C}{T - \Theta} + \chi_{dia} + \chi_p, \text{ with} \quad (1)$$

$$C = \frac{N_0 g^2 \mu_B^2 S(S+1) \bar{x}_{Mn}}{3k_B} \quad (2)$$

where C is the Curie constant, Θ is the paramagnetic Curie-Weiss temperature, $\chi_{dia} = -2 \times 10^{-7}$ emu/g is the diamagnetic contribution to the magnetic susceptibility originating from the host lattice (the value was determined from our magnetization measurements of $ZnGeAs_2$), χ_p is the paramagnetic contribution to the magnetic susceptibility originating from short-range coupled Mn-ions, N_0 is the number of cation sites per gram, $g \simeq 2$ is the effective spin-splitting factor, $S = 5/2$ is the spin-magnetic momentum of the Mn ions, μ_B is the Bohr magneton, k_B is the Boltzmann constant, and \bar{x}_{Mn} is the effective magnetically-active Mn content. The experimental $(Re(\chi_{AC}))^{-1}(T)$ curves for the temperatures higher than 20 K are fitted to Eq.1 (see Fig. 3) with the values of C , Θ , and χ_p as fitting parameters. The contribution to the magnetic susceptibility originating from the short-range-coupled Mn ions is found to be an increasing function of the Mn-content changing from the value of 3×10^{-7} emu/g up to 1.3×10^{-6} emu/g. It is a signature that the amount of paramagnetic ion pairs forming Mn-As-Mn configurations coupled with superexchange magnetic interaction increases with increasing concentration of Mn in the sample.

The fitting procedure shows that both Θ and C are highly composition dependent. The values of the Curie constant are used to calculate the magnetically-active

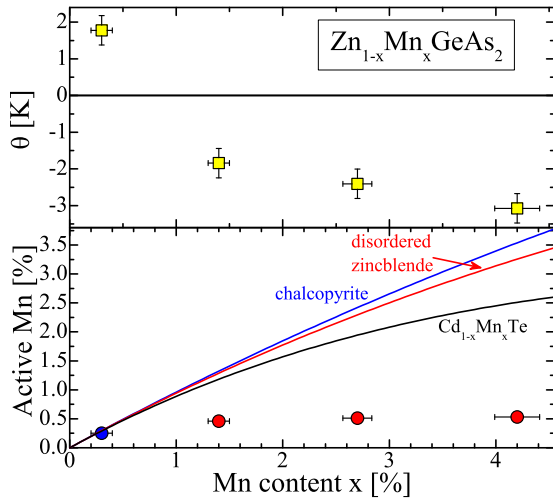


FIG. 4. The Curie-Weiss temperature and the effective magnetically-active Mn-content as a function of the chemical composition for the $Zn_{1-x}Mn_xGeAs_2$ samples. Markers - experimental data, solid lines calculated for random magnetic ions distribution (see text).

Mn-content, \bar{x}_{Mn} , using Eq. 2. As a result of the fitting procedure the values of the Curie-Weiss temperature and the amount of magnetically active Mn ions are evaluated. The results of the fitting procedure are gathered in Fig. 4. The obtained results show that the Curie-Weiss temperature changed sign with an increase of the Mn content. It indicates the change of the dominant magnetic interactions in this system from ferromagnetic at low composition x to antiferromagnetic for x between 0.003 and 0.014. It is therefore possible that, with the increase of Mn in the alloy above $x = 0.003$, the amount of Mn not diluted randomly in the crystal increases. At the same time we observe that the amount of magnetically active Mn ions, \bar{x}_{Mn} , is close to the average Mn content, x , only in the case of a very diluted $Zn_{0.997}Mn_{0.003}GeAs_2$ sample. In addition to the above mentioned sample, for all our crystals with $0.014 \leq x \leq 0.042$ the quantity of magnetically active Mn ions remaining in the state of high-spin $J = S = 5/2$ does not exceed $\bar{x}_{Mn} \approx 0.005 \pm 0.001$. It is evident, that the majority of Mn ions in $Zn_{1-x}Mn_xGeAs_2$ samples with $x \geq 0.014$ does not substitute Zn sites in the crystal lattice and therefore possess smaller net magnetic moment than Mn^{2+} . Moreover, it is also probable that a large fraction of Mn ions in these samples occupies interstitial sites of the crystal lattice, which promotes short range superexchange interactions leading to antiferromagnetic pairing of Mn ions and zero net magnetic moment of such pairs. The antiferromagnetic state of Mn ions with no net magnetic moment is energetically preferred for $Zn_{1-x}Mn_xGeAs_2$ system with $x = 0.25$ and 0.50 [19]. It is therefore highly probable that the magnetic ions form antiferromagnetic states in this semiconductor matrix when x value is higher than 0.25.

The data allow to comment on the distribution of mag-

netic Mn ions in the sample. In presence of short-range antiferromagnetic interactions a fraction of Mn ions is magnetically inactive, i.e. involved in clusters showing zero or low ground state spin (dominantly antiferromagnetically coupled pairs for low x). Therefore, the main contribution to magnetization originates from ions which do not possess nearest-neighbors in the sublattice occupied by magnetic ions and thus do not belong to clusters. If the distribution of ions within the magnetic sublattice is purely random, the amount of magnetically active ions can be estimated as $\bar{x} = x(1-x)^z$, where z is the maximum number of nearest-neighbor magnetic ions which can couple antiferromagnetically to a given ion. For typical diluted magnetic semiconductors having a zincblende structure, the corresponding formula is $\bar{x} = x(1-x)^{12}$. In case of our samples, two crystalline structures were detected, as mentioned in the section II. We assume that Mn ions couple antiferromagnetically through the superexchange mechanism via As ions. Therefore, for chalcopyrite structure, we have $\bar{x} = x(1-x)^4$. On the other hand, for a quaternary sample with a disordered zincblende structure $Zn_{1-x}Mn_xGeAs_2$ the Mn content x applies only to a half of the cations, therefore we should calculate $\bar{x} = x[1 - (x/2)]^{12}$. In Fig. 4 we plot by solid lines the estimates of active Mn content for both crystalline structures found in our samples, as well as an estimate for a classical diluted magnetic semiconductor, $Cd_{1-x}Mn_xTe$. It is visible that for $x > 0.003$, the calculated values of active Mn concentration are several times higher than those found experimentally. Such a discrepancy is a signature of the fact that Mn ions are not distributed randomly in our samples.

B. High field results

The magnetization of our samples was studied with the use of the Quantum-Design Superconductive-Quantum-Interference-Device (SQUID) magnetometer system. The SQUID magnetometer enabled precise measurements of the magnetic moment of the samples as a function of the magnetic field up to $B = 5$ T and at temperatures in the range $2 \leq T \leq 100$ K. The isothermal magnetic field dependencies of the magnetization were measured for the samples with different chemical content. The experimental results were corrected by subtracting the contribution of the sample holder. Magnetization of all the samples does not show magnetic hysteresis for temperatures above 2 K. That may indicate a lack of macroscopic MnAs precipitates and that the long-range RKKY itinerant interaction does not produce magnetic order at $T > 2$ K. The exemplary $M(B)$ curves obtained for the selected $Zn_{1-x}Mn_xGeAs_2$ samples with different chemical composition are presented in Fig. 5. The magnetization shows a diamagnetic response for nonmagnetic $ZnGeAs_2$ sample indicating the absence of non-intentional paramagnetic ion doping present in our pure sample, in agreement with previous result based on

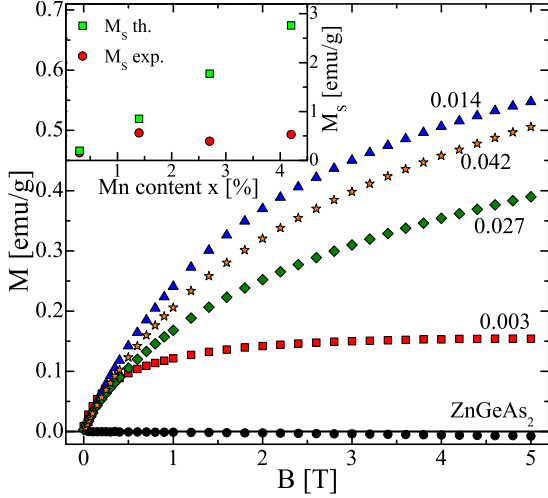


FIG. 5. The isothermal magnetic field dependencies of the magnetization measured at $T = 2$ K for our $\text{Zn}_{1-x}\text{Mn}_x\text{GeAs}_2$ samples. The inset shows the magnetization M_S exp. obtained from fitting our experimental data with Eqs. 3 and 4 (circles) and the saturation magnetization M_S th. obtained from Eq. 4 by assuming $\bar{x} = x$ (rectangles).

the susceptibility results. The magnetization curve observed for the chalcopyrite $\text{Zn}_{1-x}\text{Mn}_x\text{GeAs}_2$ sample with $x = 0.003$ shows a behavior characteristic of a paramagnet, i.e., the $M(B)$ curve can be easily fitted with the use of Brillouin function. Moreover, the saturation of the $M(B)$ curve for the sample with $x = 0.003$ is reached at the magnetic field $B \approx 3$ T. It is a signature of a random Mn-distribution in the host lattice, and preferably lack of significant antiferromagnetic Mn-pairing. The addition of higher quantity of Mn to the alloy resulted in a different shape of the $M(B)$ curve for our crystals with $x > 0.01$. As we can see in Fig. 5 the magnetization does not reach saturation even at $B = 5$ T.

We fitted our experimental data to the expression²⁸

$$M = M_S B_J \left(\frac{g\mu_B J B}{k_B(T + T_0)} \right) + \chi_{dia} B, \quad (3)$$

where

$$M_S = \bar{x} N_0 \mu_B g J, \quad (4)$$

and B_J is the Brillouin function. The term $\chi_{dia} B$ represents the diamagnetic contribution of the ZnGeAs_2 , g is the g -factor of the magnetic ion (for Mn $g = 2$), μ_B is the Bohr magneton, $J = S = 5/2$ is the total magnetic momentum of the Mn^{2+} ion, k_B is the Boltzmann constant, T is the temperature, and N_0 is the number of cation sites per gram.

The two fitting parameters, \bar{x} and T_0 , represent the amount of magnetically active Mn ions in the material and the exchange interaction among magnetic ions, respectively. The T_0 values obtained for our samples were close to the estimated Curie-Weiss temperatures, Θ , and

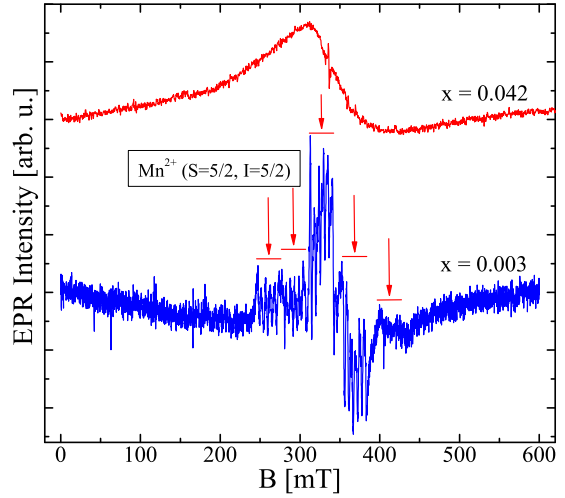


FIG. 6. The EPR spectra measured at $T = 10$ K for selected $\text{Zn}_{1-x}\text{Mn}_x\text{GeAs}_2$ samples with different chemical composition.

decreased as a function of x : for $x = 0.003$ $T_0 = 1.13$ K, for $x = 0.014$ $T_0 = -1.47$ K, for $x = 0.027$ $T_0 = -1.50$ K, and for $x = 0.042$ $T_0 = -1.95$ K. The estimated error in T_0 is about 20%.

In the inset to Fig. 5 we show the magnetization M_S th. calculated using Eq. 4 with $\bar{x} = x$ and the magnetization M_S exp. obtained from fitting our experimental data to Eqs. 3 and 4 with \bar{x} and T_0 as fitting parameters.

We used the Eqs. 3 and 4 to estimate the amount magnetically active Mn ions in our samples, \bar{x} . The calculated x/\bar{x} ratio equals to 1.28 and 1.51 for $x = 0.003$ and 0.014, respectively, and increases dramatically up to 4.5 and 5.2 for $x = 0.027$ and 0.042, respectively. It indicates rather poor Mn allocation in the $\text{Zn}_{1-x}\text{Mn}_x\text{GeAs}_2$ semiconductor matrix for $x \geq 0.014$ and that the level of frustration in the material increases as a function of x . The $M(B)$ results and their interpretation are in agreement with the susceptibility data.

C. Electron paramagnetic resonance

The electron paramagnetic resonance (EPR) spectra were measured with the use of Bruker EMX spectrometer. The sample was put into microwave radiation with fixed frequency 9.40 GHz. The temperature of the sample was controlled with the use of Oxford Instruments helium flow cryostat. The measurements performed at selected temperatures showed a signal related to the presence of Mn ions only at low temperatures around 10 K. The normalized EPR spectra obtained for two selected $\text{Zn}_{1-x}\text{Mn}_x\text{GeAs}_2$ samples are gathered in Fig. 6. Since our samples are polycrystalline the EPR results are the average over all possible directions of crystallites with respect to the external magnetic field axis. The EPR results for low Mn content $\text{Zn}_{0.997}\text{Mn}_{0.003}\text{GeAs}_2$ indicate the presence of thirty resonance lines - pattern, charac-

teristic for Mn^{2+} ions showing both fine and hyperfine structure components, due to electron spin $S=5/2$ and nuclear spin $I=5/2$, respectively. We believe that five groups, each consisting of six lines belonging to Mn^{2+} , are observed (marked in Fig. 6). The shift between the five line groups is due to the presence of zero-field-splitting of the ground state levels. Clearly, the EPR results shows the $2+$ charge state of Mn ions in the $Zn_{0.997}Mn_{0.003}GeAs_2$ sample. This interpretation would be consistent with the magnetometry data. For the $Zn_{1-x}Mn_xGeAs_2$ with Mn content higher than $x=0.003$, due to the broadening of the resonance lines, both fine and hyperfine structure of Mn^{2+} becomes unresolved. The electron effective g factor for our samples, as estimated from the EPR spectrum, equals to 1.9972.

D. Curie-Weiss temperature and determination of J_{pd}

Let us discuss the dependence of the Curie-Weiss temperature on the magnetic component concentration x for a diluted magnetic semiconductor. If both short-range antiferromagnetic couplings and long-range net ferromagnetic interactions are present in the system, the value of Θ can be written as²⁹ $\Theta = \bar{x}\Theta_F + \Theta_{AF}$, where

$$\Theta_F = \frac{S(S+1)}{3k_B} \sum_k z_k J(r_k), \quad (5)$$

and Θ_{AF} is an antiferromagnetic term, depending on x but not directly proportional, z_k is the number of lattice sites at a distance of r_k from the selected site at the origin, and $J(r_k)$ is the exchange interaction between magnetic ions separated by a distance r_k . Let us emphasize that the summation is performed only over the lattice sites which can be occupied by substitutional magnetic ions. We exclude the ions involved in nearest-neighbour pairs from the sum in Eq. 5, since we assume that they are blocked by strong short-range antiferromagnetic couplings. Using the effective concentration, \bar{x} , determined from fitting the experimental data to Eqs. 3 and 4 is based on the assumption that only this fraction of magnetic ions is magnetically active, at least in the range of applied magnetic fields and temperatures used.

For the case of the sample with the lowest Mn content ($x=0.003$), for which the Curie-Weiss temperature is positive (ferromagnetic), we made an attempt to explain the Curie-Weiss temperature value by applying a Ruderman-Kittel-Kasuya-Yosida (RKKY) model of long-range magnetic interactions. For that purpose we assume that the antiferromagnetic contribution, Θ_{AF} , is negligible due to an ultralow concentration of magnetic ions, and that only a ferromagnetic contribution to Curie-Weiss temperature exists. In our considerations, the appropriate distances and numbers of lattice sites at a given distance are generated for a chalcopyrite lattice (in which Mn ions substitute Zn ions) with lattice constants a and c discussed in the Section II.

The interaction between the magnetic ions is assumed to be the RKKY interaction for disordered three-dimensional system²⁰⁻²³:

$$J(r) = N_V \frac{J_{pd}^2 m^* a^4 c^2}{8\pi^3 \hbar^2} k_F^4 \times \frac{\sin(2k_F r) - (2k_F r) \cos(2k_F r)}{(2k_F r)^4} \exp(-r/\lambda), \quad (6)$$

where $k_F = (3\pi^2 n/N_V)$ is the Fermi wavevector and J_{pd} is the Mn-hole exchange interaction constant.

In the calculations, we assumed the effective mass of the charge carriers $m^*/m_e = 0.4$ (similar to that in GaAs) and the number of valleys $N_V = 3$. The characteristic decay length, λ , can be identified as a mean free path for the charge carriers. Such a quantity can be estimated using Drude model of conductivity from the formula $\lambda = \hbar k_F \mu / e$, where μ is the mobility of the charge carriers and e denotes elementary charge value. In order to determine the λ value we used the values of charge carrier concentration and mobility for the sample with $x=0.003$ at the lowest available temperature, i.e. about 4 K, what yielded the result of $\lambda = 10 \text{ \AA}$. For the accepted parameter values, the experimental value of $\Theta = (1.8 \pm 0.4) \text{ K}$ would yield $J_{pd} = (0.75 \pm 0.09) \text{ eV}$. Let us note that the given uncertainty in the J_{pd} value is only due to the corresponding uncertainties in the Curie-Weiss temperature and effective concentration of magnetic ions. Additionally, we mention that one of the factors influencing the determined value of exchange energy is the temperature dependence of carrier concentration and mobility (see Fig. 1). Therefore the coupling between spins is temperature-dependent. The corresponding $\Theta_F \simeq \Theta/\bar{x}$ amounts to approximately 755 K.

Let us state that in presence of both ferro- and antiferromagnetic interactions, the increase in x may result in a sign change of Curie-Weiss temperature, $\Theta = \bar{x}\Theta_F + \Theta_{AF}(x)$. The characteristic antiferromagnetic temperature, $\Theta_{AF} < 0$, is a function of magnetic component concentration x . Its dependence on x is known from experimental data for such diluted magnetic semiconductors as $Zn_{1-x}Mn_xTe$ and $Cd_{1-x}Mn_xTe$ ^{24,29}. Also, a dependence of \bar{x} is known for such alloys. In already mentioned typical DMSs, the magnetic ion distribution is found to be random and uncorrelated. We can model qualitatively the Θ sign change using the dependencies of \bar{x} and Θ_{AF} taken from^{24,30} for $Cd_{1-x}Mn_xTe$. The results are presented in Fig. 7, where predicted Curie-Weiss temperatures are plotted for various values of Θ_F , which describes the total strength of long-range ferromagnetic interactions. It is visible that in presence of moderately strong ferromagnetic interactions we observe a sign change in Θ . However, it is evident that this transition takes place for considerably higher concentrations of magnetic ions and the slope of Curie-Weiss temperature change is lower than that observed experimentally for our samples. This supports the picture of non-random

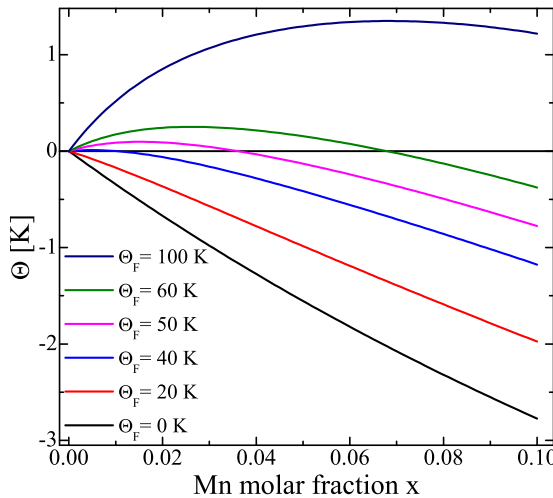


FIG. 7. The calculated Curie-Weiss temperature as a function of the Mn content, x , for selected values of the characteristic ferromagnetic temperature Θ_F , based on data for $\text{Cd}_{1-x}\text{Mn}_x\text{Te}$, a representative DMS with random distribution of magnetic impurities.

distribution of magnetic ions, with significantly stronger antiferromagnetic contribution than expected from the presented model.

On the basis of the determined value of J_{pd} , we can make an attempt to predict the characteristic temperatures Θ_F for our samples with Mn content higher than $x = 0.003$. For this purpose we take into account the low-temperature charge carrier concentrations and mobilities and we use the Eq. 6 with an assumption that J_{pd} is composition-independent. In this manner, for a sample with $x = 0.014$ we obtain $\Theta_F = 1465$ K; for $x = 0.027$ we have $\Theta_F = 165$ K and for $x = 0.042$ we get $\Theta_F = 1040$ K. Note that if the distribution of Mn ions would be random in those samples, then the values of $\bar{x}\Theta_F$ would be high. Having the experimental values of Curie-Weiss temperatures, we can estimate the characteristic parameters Θ_{AF} for our samples from $\Theta = \bar{x}\Theta_F + \Theta_{AF}$. As a consequence, we get the values of Θ_{AF} equal to -15.4 K, -3.4 K and -11.4 K for the samples with $x = 0.014$, $x = 0.028$ and $x = 0.042$, accordingly. The characteristic antiferromagnetic temperatures are quite high in magnitude (especially when compared, for example, with the values for $\text{Cd}_{1-x}\text{Mn}_x\text{Te}$ ^{24,30}). This fact supports the conclusion that the distribution of Mn

ions in our samples is far from random and that the tendency towards creation of antiferromagnetically coupled clusters is promoted.

V. SUMMARY

We explored the structural, electrical, and magnetic properties of low-Mn-dilution limit of $\text{Zn}_{1-x}\text{Mn}_x\text{GeAs}_2$ alloy with $0 \leq x \leq 0.042$. The XRD results indicate the appearance of chalcopyrite and disordered zincblende structure in our samples, strongly Mn content dependent.

The transport characterization shows that all our samples have high p type conductivity with carrier concentration $n > 10^{19} \text{ cm}^{-3}$ and mobility $\mu < 50 \text{ cm}^2/(\text{V}\cdot\text{s})$. The magnetoresistance in our samples shows large values, up to -50%, for $\text{Zn}_{0.997}\text{Mn}_{0.003}\text{GeAs}_2$. The values are not correlated with magnetic properties of the alloy. We believe the the MR in our samples is due to weak localization phenomena.

The magnetic properties of the alloy indicate that in the case of the sample with very low Mn content, $x = 0.003$, the majority of Mn ions is in a high-spin Mn^{2+} charge state. For the samples with higher Mn content a large fraction of Mn ions forms antiferromagnetic pairs and/or clusters and stays in other, low moment charge states. The Curie-Weiss temperature, as determined from low-temperature magnetic susceptibility data, has small values $|\Theta| < 3$ K and changes sign from positive for $x = 0.003$ into negative for higher Mn content. The Mn-hole exchange integral, estimated for the very diluted $\text{Zn}_{0.997}\text{Mn}_{0.003}\text{GeAs}_2$ sample is equal to $J_{pd} = (0.75 \pm 0.09)$ eV indicating rather strong magnetic interactions in this material.

VI. ACKNOWLEDGMENTS

Scientific work was financed from funds for science in 2011-2014, under the project no. N202 166840 granted by the National Center for Science of Poland. This work has been supported by the Polish Ministry of Science and Higher Education on a special purpose grant to fund the research and development activities and tasks associated with them, serving the development of young scientists and doctoral students.

* kilan@ifpan.edu.pl

¹ J. Kossut and W. Dobrowolski, Handbook of Magnetic Materials (North-Holland, Amsterdam, 1993), Vol. 7, pp. 231305.

² W. Dobrowolski, J. Kossut, and T. Story, Handbook of Magnetic Materials (Elsevier, New York, 2003), Vol. 15, Chaps. IIVI and IVVI, pp. 289377.

³ S. C. Erwin and I. Žutić, *Nature Materials* **3**, 410 (2004).

⁴ S. Picozzi, *Nature Materials* **3**, 349 (2004).

⁵ L. Kilanski, M. Górska, V. Domukhovski, W. Dobrowolski, J. R. Anderson, C. R. Rotundu, S. A. Varniavskii, and S. F. Marenkin, *Acta Phys. Pol. A* **114**, 11511157 (2008).

⁶ L. Kilanski, A. Zubiaga, F. Tuomisto, W. Dobrowolski, V. Domukhovski, S. A. Varniavskii, and S. F. Marenkin, *J.*

Appl. Phys. **106**, 013524 (2010).

⁷ L. Kilanski, M. Górska, W. Dobrowolski, E. Dynowska, M. Wójcik, B. J. Kowalski, J. R. Anderson, C. R. Rotundu, D. K. Maude, S. A. Varnavskiy, I. V. Fedorchenko, and S. F. Marenkin, *J. Appl. Phys.* **108**, 073925 (2010).

⁸ H. Ohno, *Science* **281**, 951 (1998).

⁹ L. Kilanski, I. V. Fedorchenko, M. Górska, E. Dynowska, M. Wójcik, B. J. Kowalski, J. R. Anderson, C. R. Rotundu, S. A. Varnavskiy, W. Dobrowolski, and S. F. Marenkin, *Phys. Stat. Sol. B* **248**, 1601 (2011).

¹⁰ M. Romčević, N. Romčević, W. Dobrowolski, L. Kilanski, J. Trajić, D. V. Timotijević, E. Dynowska, I. V. Fedorchenko, S. F. Marenkin, *J. Alloys Compd.* **33**, 548 (2013).

¹¹ V. M. Novotortsev, V. T. Kalinnikov, L. I. Koroleva, R. V. Demin, S. F. Marenkin, T. G. Aminov, G. G. Shabunina, S. V. Boichuk, and V. A. Ivanov, *Russ. J. Inorg. Chem.* **50**, 492 (2005).

¹² W. J. Paszkowicz, *J. Appl. Crystallogr.* **22**, 186 (1989).

¹³ S. Schön, M. L. Fearheiley, K. Diesner, and S. Fiechter, *J. Cryst. Growth* **135**, 601 (1994).

¹⁴ C. Rincón, *Phys. Rev. B* **45**, 12716 (1992).

¹⁵ P. W. Anderson, *Phys. Rev.* **109**, 1492 (1958).

¹⁶ P. G. de Gennes and J. Friedel, *J. Phys. Chem. Solids* **4**, 71 (1958).

¹⁷ T. Moriya and A. Kawabata, *J. Phys. Soc. Jpn.* **34**, 639 (1973).

¹⁸ T. Moriya and A. Kawabata, *J. Phys. Soc. Jpn.* **35**, 669 (1973).

¹⁹ Y. Zhao, S. Picozzi, A. Continenza, W. T. Geng, and A. J. Freeman, *Phys. Rev. B* **65**, 094415 (2002).

²⁰ M. A. Ruderman, and C. Kittel, *Phys. Rev.* **96**, 99 (1954).

²¹ T. Kasuya, *Progr. Theor. Phys.* **16**, 45 (1956).

²² K. Yosida, *Phys. Rev.* **106**, 893 (1957).

²³ P. G. de Gennes, *J. Phys. Radium* **23**, 630 (1962).

²⁴ J. Cibert, and D. Scalbert, in: *Spin Physics in Semiconductors* (Springer, Berlin, 2008), ed. by M. I. Dyakonov, Chap. 13, p. 389.

²⁵ R. A. Lee and T. V. Ramakrishnan, *Rev. Mod. Phys.* **57**, 287 (1985).

²⁶ D. V. Baxter, R. Richter, M. L. Trudeau, R. W. Cochrane and J. O. Strom-Olsen, *J. Phys. France* **50**, 1673 (1989).

²⁷ A. Lewicki, A. I. Schindler, I. Miotkowski, and J. K. Furdyna, *Phys. Rev. B* **41**, 4653 (1990).

²⁸ J. A. Gaj, R. Planel, and G. Fishman, *Solid State Commun.* **29**, 435 (1979).

²⁹ D. Ferrand, J. Cibert, A. Wasiela, C. Bourgognon, S. Tatarenko, G. Fishman, T. Andrearczyk, J. Jaroszyński, S. Koleśnik, T. Dietl, B. Barbara, and D. Dufeu, *Phys. Rev. B* **63**, 085201 (2001).

³⁰ J. A. Gaj, W. Grieshaber, C. Bodin-Deshayes, J. Cibert, G. Feuillet, Y. Merle d'Aubigné, and A. Wasiela, *Phys. Rev. B* **50**, 5512 (1994).